García-Fernández, A.; García-Laínez, G.; Ferrandiz Manglano, ML.; Aznar, E.; Sancenón Galarza, F.; Alcaraz, MJ.; Murguía, JR.... (2017). Targeting inflammasome by the inhibition of caspase-1 activity using capped mesoporous silica nanoparticles. Journal of Controlled Release. 248:60-70. doi:10.1016/j.jconrel.2017.01.002

Targeting inflammasome by the inhibition of caspase-1 activity using capped mesoporous silica nanoparticles

Alba García-Fernández,[a,b,c], Guillermo García-Laínez,[d] María Luisa Ferrándiz,[a,e] Elena Aznar,[a,b,c] Félix Sancenón,[a,b,c] María José Alcaraz,[a,e,] José Ramón Murguía,[a,b,c] María D. Marcos,[a,b,c] Ramón Martínez-Máñez,[a,b,c,*] Ana M. Costero,[a,c,f] and Mar Orzáez,[d],**

AUTHOR EMAIL ADDRESS rmaez@qim.upv.es

* To whom correspondence should be addressed: Ramón Martínez-Máñez: Phone: 34-963877343; Fax: 34-963879349.

[a] Instituto Interuniversitario de Investigación de Reconocimiento Molecular y Desarrollo Tecnológico (IDM). Universitat Politècnica de València, Universitat de València, Spain. Camino de Vera s/n. Valencia 46022, Spain

[b] Departamento de Química. Universitat Politècnica de València. Camino de Vera s/n, Valencia 46022, Spain.

[c] CIBER de Bioingeniería, Biomateriales y Nanomedicina (CIBER-BBN). Spain.

[d] Centro de Investigación Príncipe Felipe. Eduardo Primo Yúfera, 3. Valencia 46012, Spain.

[e] Departamento de Farmacología, Facultat de Farmàcia. Universitat de València, Av. Vicente Andrés, s/n. 46100 Burjassot, Valencia, Spain.

[f] Departamento de Química Orgánica. Universitat de València, Dr Moliner 50, 46100, Burjassot, Valencia, Spain.

Abstract

Acute inflammation is a protective response of the body to harmful stimuli, such as pathogens or damaged cells. However, dysregulated inflammation can cause secondary damage and could thus contribute to the pathophysiology of many diseases. Inflammasomes, the macromolecular complexes responsible for caspase-1 activation, have emerged as key regulators of immune and inflammatory responses. Therefore, modulation of inflammasome activity has become an important therapeutic approach. Here we describe the design of a smart nanodevice that takes advantage of the passive targeting of nanoparticles to macrophages and enhances the therapeutic effect of caspase-1 inhibitor VX-765 *in vivo*. The functional hybrid systems consisted of MCM-41-based nanoparticles loaded with anti-inflammatory drug VX-765 (S2-P) and capped with poly-L-lysine, which acts as a molecular gate. S2-P activity has been evaluated in cellular and *in vivo* models of inflammation. The results indicated the potential advantage of using nanodevices to treat inflammatory diseases.

Keywords

Gated mesoporous silica nanoparticles, controlled release, inflammasome, VX-765, macrophages, air pouch mouse model.

1. Introduction

The use of gated materials in biomedical applications has increased in the past few years thanks to their ability to release therapeutic drugs upon the application of external stimuli. These nanodevices have attracted much attention as candidates for the development of potential new therapies to improve drug efficacy and safety, and are potential alternatives to liposomes and polymeric carriers, which usually release their cargo via simple diffusion-controlled processes or through container degradation [1-7]. Gated nanoparticles have been used for controlled delivery applications since the first report by Fujiwara and co-workers [8, 9]. To date, several examples of gated systems capable of delivering their cargo have been described [10] upon the application of specific chemical [11-14] physical [15-17] and biochemical [18-20] stimuli.

The unique properties of mesoporous silica nanoparticles (MSNs), such as large loading capacity, low toxicity, stability, biocompatibility and easy functionalization, make them most appealing as carriers for drug storage and on-command delivery [21-23]. Moreover, gated MSNs are also suitable nanocarriers of poor soluble drugs and are able to protect drugs from degradation [24-27]. The combination of the remarkable properties of MSNs as nanocarriers and the use of polymers as caps has been proven a feasible procedure to develop drug delivery systems for applications in a more biological and realistic environment. In this subfield of research, several examples have been reported in the literature on MSNs with polymers capable of delivering the payload by changes in temperature, pH, redox activity and by presence of target enzymes [10] [28].

From another point of view, the intrinsic capacity of macrophages to internalize foreign bodies evidences their potential use for targeting drug delivery using nanoparticles [29-31]. Accordingly, efforts made to develop innovative therapies have been reported that use nanomaterials as intramacrophagic vectors to enhance the antimicrobial effects of antibiotics, based mainly on liposomes [32, 33], polymeric [34, 35] and carbon nanotube [36, 37] carriers. While the use of liposomes, solid lipid particles and biodegradable nanoparticles has been described to target macrophages and deal with infectious diseases, the use of gated silica nanoparticles as a delivery platform to manage inflammation by taking advantage of targeting passive for macrophages has not been previously reported. Very few recent reports have been found that describe the use of MSNs in the inflammation field that lead to infectious diseases [38] and neuroinflammation [39].

Macrophages are cells implicated in host defense that attack harmful substances through destruction and ingestion associated with an inflammatory response to limit harm to the body [40]. Dysregulated macrophage function and, thus dysregulated inflammation, have been implicated in the pathophysiology of a wide range of disorders, including chronic ulcers, allergic asthma, atherosclerosis, autoimmune disorders and fibrotic diseases, Alzheimer's disease, etc. [41]. Inflammation initiates upon the sensing of signs of acute damage or disturbances in tissue homeostasis, which results in the synthesis and activation of potent pro-inflammatory cytokines, such as pro-Interleukin-1 beta (pro-IL-1β) [42]. This activation is a proteolytic process controlled by interleukin-1 beta (IL-1β)-converting enzyme, caspase-1, which cleaves key pro-inflammatory cytokine IL-1β to trigger inflammation [43]. The protein

complexes responsible for caspase-1 activation are inflammasomes [44]. Inflammasomes are molecular platforms formed by an inflammasome sensor molecule (the NLR protein), adaptor protein ASC and protease caspase-1. The formation of these multiprotein oligomers activates caspase-1 that triggers the maturation of pro-inflammatory cytokines IL-1β and IL-18 [45]. Another consequence of caspase-1 activation in macrophages is a pro-inflammatory form of caspase-1-dependent cell death, known as pyroptosis [46, 47]. Alterations in inflammasome components are involved in the physiopathology of several of the above-mentioned inflammatory diseases [48]. Therefore, modulation of inflammasome activity is an important target to develop effective therapeutics to treat inflammation and related inflammatory diseases.

One emerging strategy to treat inflammatory diseases consists of drugs that target caspase activity. One specific inhibitor of caspase-1 is VX-765, a prodrug converted efficiently into the potent and selective inhibitor of ICE/caspase-1 VRT-043198 with the action of esterases. The therapeutic effect of this drug has already been demonstrated in preclinical studies and clinical trials to treat inflammatory and autoimmune conditions. Former studies have shown their therapeutic potential effect by reducing disease severity and inflammatory response in mouse models of rheumatoid arthritis and skin inflammation. Reducing cytokines production by inhibiting caspase-1, using drugs like VX-765, is a promising approach to consider the important role of these cytokines in inflammatory diseases [49, 50].

Here we report the synthesis, characterization and controlled release behavior of gated-MSNs in both *in vitro* and *in vivo* models of inflammation. MSNs nanodevices were loaded with rhodamine B (S1) or drug VX-765 (S2),

and were capped with polymer ε-poly-L-lysine. Nanoparticles showed “zero release”, yet cargo was delivered in the presence of a target stimulus (presence of pronase enzymes). Nanoparticles’ behavior was studied in the THP-1 acute monocytic leukemia cell line stimulated, or not, with lipopolysaccharide (LPS) and muramyl dipeptide (MDP) to produce the synthesis of pro-IL1-β and the activation of pro-caspase-1 by the inflammasome. Capped nanoparticles were also evaluated in a subcutaneous air pouch inflammation mouse model.

2. Materials and methods

2.1. General methods.

Powder X-ray diffraction (PXRD), thermogravimetric analysis (TGA), transmission electron microscopy (TEM), N_2 adsorption-desorption and elemental analyses were run to characterize synthesized materials. PXRD measurements were taken with a Philips D8 Advance Diffractometer using CuKα radiation. TGAs were carried out on a TGA/SDTA 851e Mettler Toledo balance in an oxidant atmosphere (air, 80 mL/min) with a heating program that consisted of a heating ramp of 10°C per minute from 25ºC to 100ºC. Then the temperature was kept at 100ºC for 60 min. Finally, a new heating ramp of 10ºC per minute from 100ºC to 1000ºC was applied and an isothermal heating step at the final temperature for 30 min. TEM images were obtained under a 100 KV JEM-1010 microscope. N_2 adsorption-desorption isotherms were recorded with a Micromeritics ASAP2010 automated sorption analyzer. Samples were degassed at 120°C in vacuum overnight. Specific surface areas were calculated from the adsorption data within the low pressure range using the BET model. Pore size was determined following the BJH method. To determine the zeta potential of the bare and functionalised MSPs, a Zetasizer Nano ZS equipment

(Malvern Instruments, Malvern, UK) was used. Samples were dispersed in distilled water at a concentration of 1 mg/mL. Before each measurement, samples were sonicated for 2 min to preclude aggregation. The zeta potential was calculated from the particle mobility values by applying the Smoluchowski model. The average of five recordings was reported as zeta potential. The measurements were performed at 25ºC and performed in triplicate. Dynamic light scattering (DLS) studies for the determination of particle size were conducted at 25ºC in a Malvern Zetasizer Nano ZS instrument; all the measurements were taken in triplicate on previously sonicated highly dilute water dispersions. Fluorescence spectroscopy was carried out with a JASCO spectrofluorometer FP-8300. HPLC analyses were performed with a Merck Hitachi L-2130 HPLC pump and an L-2200 autosampler using a Lichrospher® 100 C18 (150 x 3.9 mm) column, and different acetonitrile gradients in aqueous 0.1 % TFA as the mobile phase. Live cellular internalization studies were carried out with a Cytomics FC 500 (Beckman Coulter, Inc.). Cell viability and fluorescence spectroscopy measurements were taken with a Wallac 1420 workstation. Silicon determination in mice was made by ICP-MS 7900 from Agilent.

2.2. Chemicals.

Chemicals tetraethylorthosilicate (TEOS), *n*-cetyltrimethylammonium bromide (CTABr), sodium hydroxide, (3-isocyanatopropyl)triethoxysilane, rhodamine B, trimethylamine, dimethyl sulfoxide (DMSO) and the pronase enzyme from *Streptomyces griseus* were purchased from Sigma Aldrich Química (Madrid, Spain). VX-765 was provided by AdooQ Bioscience. ε-Poly-L-lysine was purchased from Chengdu Jinkai Biology Engineering CO., Ltd. All

the other reagents were of a general laboratory grade and were purchased from Merck, unless otherwise stated. For the cell biology studies, RPMI-1640, fetal bovine serum (FBS), Dulbecco's phosphate-buffered saline (PBS), lipopolysaccharides (LPS) from *Escherichia coli* 055:B55 (*in vitro* experiments), 0111:B4 (*in vivo* experiments), adenosine 5'- triphosphate disodium salt (ATP), *N*-Acetylmuramyl-L-alanyl-D-isoglutamine hydrate (MDP), peroxidase conjugate goat anti-rabbit and anti-mouse and tetramethylammonium hydroxide (TMAH) solution 25% wt were obtained from Sigma Aldrich. Cell proliferation reagent WST-1 was obtained from Roche Applied Science (Madrid, Spain). LDH activity was measured by the Lactate Assay Kit II by BioVision. The human IL-1β ELISA Set II and skin milk powder were purchased from BD Biosciences. The caspase-1 (2225) and cleaved caspase-1 antibodies (4199) were purchased from Cell Signaling, while the α-tubulin antibody (#T8203) was obtained from Sigma-Aldrich. ECL Western blotting detection reagents were purchased from Amersham Pharmacia Biotech. Mouse IL-1β ELISA and TNF-α ELISA were purchased from R&D Systems (Minneapolis, MN, USA) Mouse IL-18 Platinum ELISA and Mouse IL-10 ELISA Ready-Set-Go were purchased from eBioscience.

2.3. Synthesis of gated mesoporous silica nanoparticles

2.3.1. Synthesis of MCM-41 mesoporous silica nanoparticles (MSNs).

CTABr (1.00 g, 2.74 mmol) was dissolved in 480 mL of deionized H_2O before adding a solution of NaOH (3.5 mL, 2.00 M). The solution temperature was adjusted to 80°C and then TEOS (5.00 mL, 2.57×10^{-2} mol) was added dropwise to the surfactant solution at maximum stirring. The mixture was stirred for 2 h to give a white precipitate. The solid was isolated by centrifugation and

washed with deionized H_2O until a neutral pH was obtained. Finally, the solid was dried at 60°C. To prepare the final porous material, MSNs were calcined at 550°C in an oxidant atmosphere to remove the template phase.

2.3.2. Synthesis of S1.

In a typical synthesis, calcined MCM-41 nanoparticles (200 mg) and rhodamine B (76.64 mg, 0.16 mmol, 0.8 mmol/g solid) were suspended in CH_3CN (7 mL). The suspension was stirred at room temperature for 24 h. Then an excess of (3 isocyanatopropyl)triethoxysilane (200 µl, 0.85 mmol, 4.25 mmol/g solid) was added, and the final mixture was stirred at room temperature for 5.5 h. The resulting pink solid (S1) was finally isolated by centrifugation, washed twice with CH_3CN (5 mL) and dried at 37°C. Taking into account the amount of rhodamine B used and the content in the loaded solid (see Table 2) a load efficiency of 54% was calculated.

2.3.3. Synthesis of S1-P.

First, S1 (200 mg) and ε-poly-L-lysine (200, mg, 1 mmol, 5 mmol of polymer/g solid) were dissolved in CH_3CN (9 mL) and H_2O (4 mL), followed by the addition of rhodamine B (50 mg) to avoid dye delivery from pores. Triethylamine (400 µl) was added and the final mixture was stirred for 2 h. Nanoparticles were centrifuged and washed thoroughly with water. The resulting solid S1-P was dried at 37ºC.

2.3.4. Synthesis of S2.

First calcined MSNs (1 g) and VX-765 (80, mg, 0.16 mmol, 0.16 mmol/g solid) were suspended in 10 mL of DMSO (VX-765 solubility in DSMO at 10

mg/mL). The suspension was stirred at room temperature for 24 h to yield solid S2. Then excess (3 isocyanatopropyl)triethoxysilane (1 mL, 4.25 mmol, 4.25 mmol/g solid) was added to a suspension that contained solid S2 (1 g) in CH_3CN (25 mL).The final mixture was stirred at room temperature for 5.5 h and the resulting white solid (S2) was isolated by centrifuging, washed twice with CH_3CN (5 mL) and dried at 37ºC. Taking into account the amount of VX-765 used and the content in the loaded solid (see Table 2) a load efficiency of 81% was calculated.

2.3.5. Synthesis of S2-P.

First, S2 (1 g) and ε-poly-L-lysine (1 g, 5 mmol, 5 mmol of polymer/g solid) were dissolved in a mixture of CH_3CN (50 mL) and H_2O (30 mL). Triethylamine (1.6 mL) was added, and the final mixture was stirred for 5.5 h. Nanoparticles were centrifuged and washed thoroughly with water. The resulting solid S2-P was dried at 37ºC.

2.4. Cargo release studies.

To investigate the stimuli-responsive gating properties of the solid, rhodamine B and VX-765 delivery studies were performed in each case in water and in a highly competitive media (PBS buffer).

In a first step, 2 mg of S1-P were placed in 1 mL of water at pH 8, and separated into two aliquots of 500 µl. Both samples were added to a volume of 2.5 mL of water at pH 8 in the absence or presence of the pronase enzyme (0.12 mg/mL) from *Streptomyces Griseus*, respectively. Suspensions were stirred at 37ºC. At certain time aliquots were separated and centrifuged to eliminate the solid and dye delivery was monitored by the fluorescence

emission band of rhodamine B at 575 nm (λ_{ex} = 555 nm) in the aqueous phase. In a second step, studies in PBS were also performed. In this case, 2 mg of S1-P were placed in 1 mL of PBS 1X at pH 7.5, and separated into two aliquots of 500 µl. Both samples were added to a volume of 2.5 mL of PBS at pH 7.5 in the absence or presence of the pronase enzyme (0.12 mg/mL) from *Streptomyces Griseus*, respectively. In addition, experiments with denatured pronase (0.12 mg/mL) were also performed to assess the role played by the enzyme in the gating mechanism of S1-P. Suspensions of S1-P in PBS were stirred at 37ºC. At certain time aliquots were separated and centrifuged to eliminate the solid and dye delivery was monitored by the fluorescence emission band of rhodamine B at 575 nm (λ_{ex} = 555 nm) in the aqueous phase.

In the S2-P delivery studies, 10 mg of the solid were suspended in 2 mL of water at pH 8. The suspension was separated into two aliquots and each was added to 4 mL of water at pH 8 in the absence or presence of the pronase enzyme (0.12 mg/mL) from *Streptomyces Griseus*, respectively. Suspensions were stirred at 37ºC. At certain time aliquots were separated and centrifuged to eliminate the solid. Drug delivery was monitored by analytical RP-HPLC with a UV detector using a mobile phase of CH_3CN-H_2O mixtures that contained 0.1% TFA at 1mL/min. Compound VX-765 was monitored at 220 nm.

2.5. Cell culture conditions.

THP-1 human leukemic monocyte cells were purchased from the German Resource Centre for Biological Materials (DSMZ) and were grown in RPMI-1640 supplemented with 10% of FBS. Cells were incubated at 37ºC in an atmosphere of 5% carbon dioxide and 95% air, and underwent passage twice a

week. For the experiments, THP-1 cells were seeded at 10^6 cell/mL in RPMI-medium at 1% of FBS.

2.6. Cytotoxicity cell assays.

THP-1 cells were seeded in a 96-well plate and treated at different S1-P concentrations (0 (control), 25, 50, 100 and 150 µg/mL in PBS). Cells were incubated for 6 h and 24 h, and then viability was determined by a WST-1 assay and a lactate dehydrogenase (LDH) activity assay. For cell viability, WST-1 was added for 30 min and then absorbance was measured at 595 nm. The cytotoxicity of mesoporous silica nanoparticles against THP-1 was addressed by measuring the LDH activity in cell culture supernatants with the Lactate Assay Kit II following the manufacturer's instructions. In this case cells were treated with 1% triton-X100, in the absence of nanoparticles, as a control positive of the LDH activity.

2.7. Cellular uptake.

In a first step, flow cytometry experiments were carried out to test the uptake of nanoparticles by THP-1 cells. For this purpose, cells were seeded in a 6 well-plate and treated with S1-P at the 0 (control), 25 and 50 µg/mL concentrations (in PBS) for 30 min. Then cells were washed with PBS and quantification of rhodamine B fluorescence was performed by flow cytometry and analyzed using version 2.9 of the WinMDI program. To assess S1-P nanoparticle's uptake by THP-1 cells, studied were carried out by confocal microscopy by means of rhodamine B associated fluorescence. THP-1 cells were seeded in a 6-well assay and treated with 50 µg/mL of nanoparticles and incubated at 37ºC for 1h. Then, cells were washed several times with PBS, and the fluorescence intensity

was monitored using a Leica TCS SP2 confocal microscope. Two independent experiments that contained triplicates were performed.

Finally, a solid containing covalently attached fluorescein was prepared and internalization studies were performed by flow cytometry and confocal microscopy as described above (see supporting information Fig.S2).

2.8. VX-765 loaded nanoparticles activity cellular assays.

Inhibition of inflammatory response by S2-P was studied in THP-1 human leukemic monocyte cells. For this purpose, cells were seeded in a 6-well plate and were then treated with S2-P at the 0 (control), 50, 75 and 100 µg/mL concentrations (in PBS). Free VX-765 was used as a reference at 1 and 2 µM (in DMSO) and with S2-P at 100 µg/mL as a nanoparticles control, respectively. After 30 min, NLPR-3 inflammasome was activated with lipopolysaccharide (LPS) from *Escherichia coli* (100 ng/mL) and muramyl dipeptide (MDP) (50 µg/mL) stimulus, and was incubated for 6 h. Finally, the cell suspension was centrifuged and separated into the supernatant and pellet.

The amount of IL-1β secreted in the cell culture supernatants of THP-1 was measured by an enzyme-linked immunosorbent assay (ELISA) kit in accordance with the manufacturer's instructions (Human IL-1β ELISA Set II from BD Biosciences).

Western blot analyses were performed to detect the amount of active caspase-1 secreted into supernatants. Samples were concentrated by methanol/chloroform precipitation [51]. To determine the amount of pro-caspase

1 as a control, whole cell extracts were obtained by lysing cells in a buffer that contained 25 mM Tris-HCl pH 7.4, 1 mM EDTA, 1 mM EGTA, and 1% SDS, plus protease and phosphatase inhibitors. Supernatants and lysates were resolved by SDS-PAGE, transferred to nitrocellulose membranes, blocked with 5% non-fat milk, washed with 0.1% Tween/PBS and incubated overnight with a specific primary antibody against caspase 1 and cleaved caspase 1 (2225 C1 and 4199 cleaved C1 from Cell Signalling). α-Tubulin was detected in cell lysates as the reference control. Membranes were washed and probed with the appropriate secondary antibody conjugated with horseradish peroxidase for enhanced chemiluminescence detection.

2.9. Characterization of the ε-poly-L-lysine-capped nanoparticles activity in *in vivo* models of inflammation.

All the studies were performed in accordance with European Union regulations for the handling and use of laboratory animals. Protocols were approved by the institutional Animal Care and Use Committee. Air pouches were produced by subcutaneous injections of 10 mL of sterile air into the back of male C57BL/6J mice (25-30 g). Three days later, 5 mL of sterile air were injected into the same cavity. Six days after the formation of air pouches, inflammation was induced by an injection of 1 mL of LPS (1µg/mL) into physiological saline [52-54].

As a preliminary assay to test the activity of the solid, gated nanoparticles and free VX-765 were injected locally into the air pouch. Mice were treated with S2-P at 0.8 and 1.6 mg/kg or with the reference VX-765 at 0.008 mg/kg (in 0.5 mL PBS + 0.1% DMSO). Air pouches in the control mice were treated with

sterile physiological saline and 0.5 mL of PBS + 0.1% DMSO. Two hours after injecting LPS, mice were killed by cervical dislocation and the exudate in the pouch was collected with 1 mL of sterile physiological saline. After centrifuging exudates, supernatants were used to measure the amount of IL-1β, IL-18, IL-10 and TNF-α by ELISA kit according to the manufacturer's instructions.

Then the same experiment was performed systemically by intravenous tail injection of nanoparticles and free drug. S2-P was injected at 75 mg/kg and VX-765 at 10 mg/kg (in 0.150 mL PBS + 0.1% DMSO). Control mice were treated with 0.150 mL of vehicle. In this case supernatants were used to measure the amount of IL-1β and IL-18. One part of the exudate sample from the blank and the mice treated with LPS and S2-P was used to study the presence of silica nanoparticles at the inflammation focus.

To determine the effect of targeting, presence of MSNs was determined by measuring the amount of silicon in the exudate from the air pouches by ICP-MS, which obtained the exudate, as described above, of three groups of mice. A control group was treated with 0.150 mL of vehicle, a second group was treated with S2-P (75 mg/kg, intravenous) and a third group with the LPS stimulus (1 μg/mL, subcutaneous) and S2-P (75 mg/kg, intravenous). Then 100 μl of air pouch exudate were introduced into 15 mL of polytetrafluoroethylene (PTFE) tubes and 1 mL of TMAH 25% was added. The digestion temperature was set at 80°C and was kept for 2 h. After cooling digests were diluted to 10 mL in polystyrene tubes. Finally 0.5 mL of the samples was diluted in a mixture of 10 mL of nitric acid 2% and hydrochloric acid 1%, and was measured in the 7900 ICP-MS in H_2 mode using germanium as an internal standard.

3. Results and discussion

3.1. Gated materials.

As stated above, the combination of polymers and MSNs is an appealing approach to design gated nanocarriers for controlled release applications. In this context we used ε-poly-L-lysine as the capping system in MSNs as a suitable polymer anchored covalently to the silica surface in order to develop gated nanodevices capable of selectively releasing the cargo (rhodamine B or VX-765) in the presence of a target stimulus (pronase enzymes). A representation of the designed nanoparticles is provided in Scheme 1.

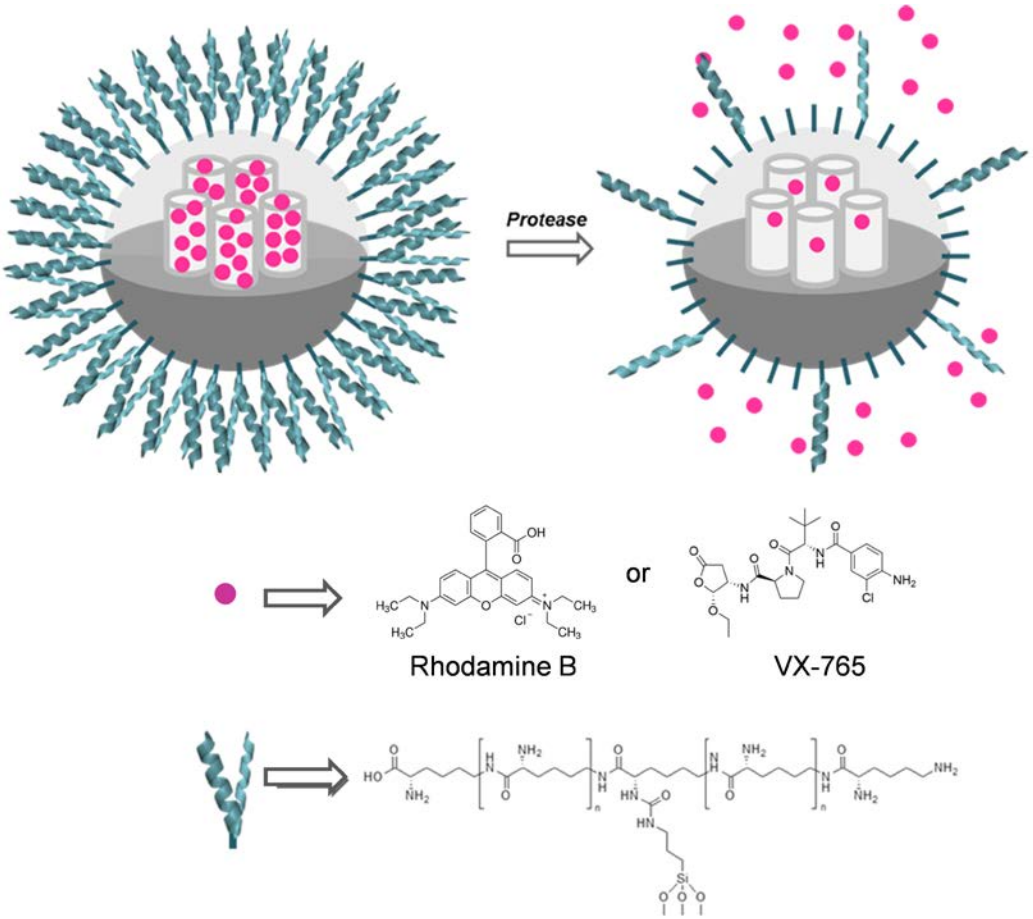

Scheme 1. Representation of the prepared gated material capped with randomly attached ε-poly-L-lysine.

MSNs were obtained following well-known procedures, loaded with the corresponding cargo and functionalized with 3-(triethoxysilyl)propyl isocyanate (solids S1 loaded with rhodamine B and S2 loaded with VX-765, see the Experimental Section). Another reaction with ε-poly-L-lysine allowed pores to be capped via the formation of urea bonds between the isocyanate groups in the nanoparticles and amine groups in the polymer (see Scheme 1) [55]. Following this simple procedure, solids S1-P and S2-P were obtained.

3.2. Characterization of nanoparticles.

The prepared solids were characterized by standard procedures. The powder X-ray patterns (PXRD) of the as-synthesized MCM-41, MCM-41 calcined, S1, S1-P and S2-P nanoparticles are shown in Figure 1. The X-ray pattern of the as-synthesized MCM-41 solid presents the four mesoporous characteristic low-angle peaks of a hexagonal-ordered array, which can be indexed as (100), (110), (200) and (210) Bragg reflections. A significant shift of (100) reflection is observed in the MCM-41 calcined nanoparticles pattern, which corresponds to an approximate cell contraction of 4 Å induced by the condensation of silanol groups in the calcination step. In the PXRD pattern of solid S1-P and S2-P, a slight intensity reduction in the (100) reflection and loss of the (110) and (200) reflections (especially for S2-P) are observed, most likely due to the reduced contrast after the loading/functionalization process. Nevertheless, the permanence of the (100) reflection in the X-ray patterns

strongly evidences that the mesoporous scaffold is maintained in the final gated nanoparticles.

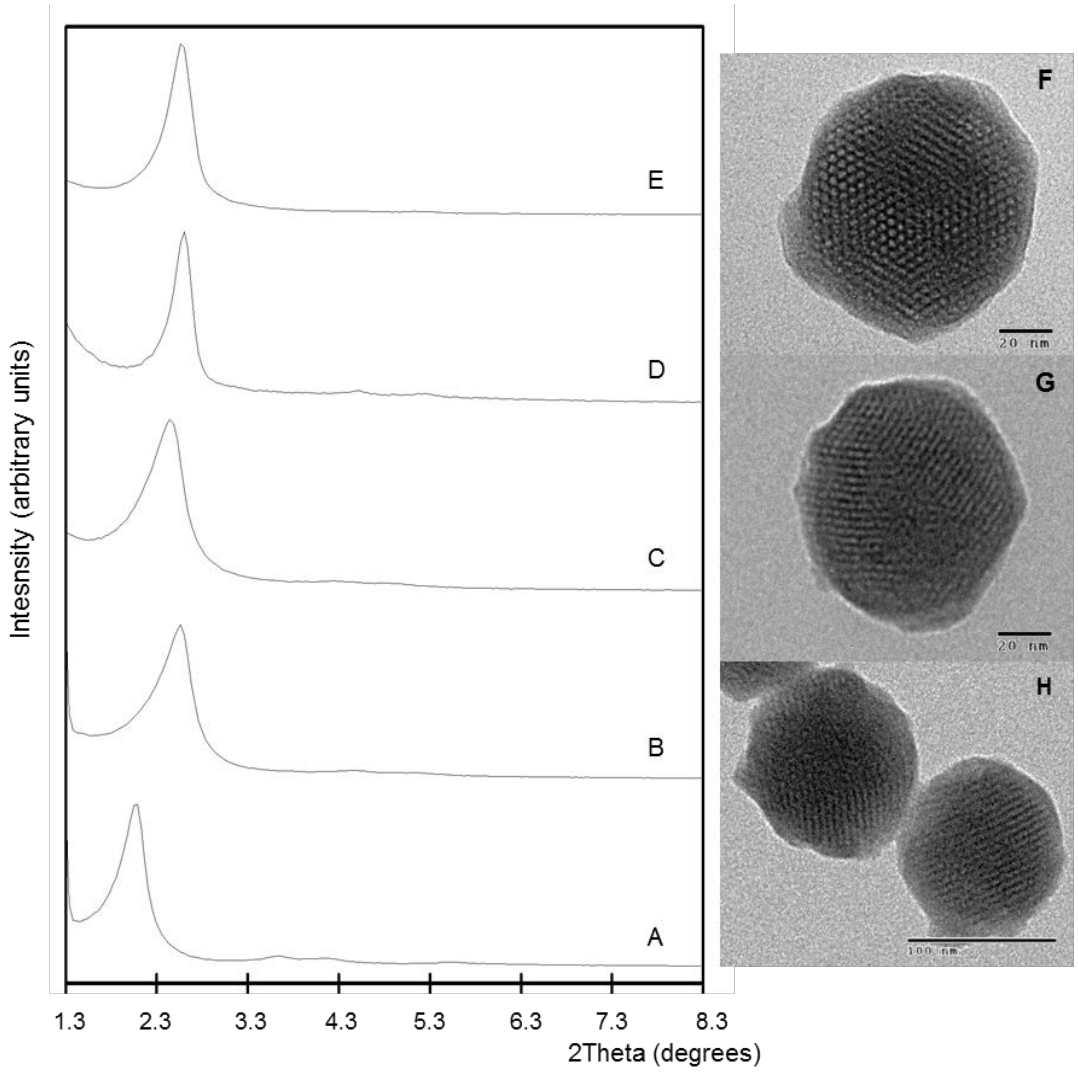

Fig. 1. Powder X-ray patterns of solids A) as-synthesized MCM-41 nanoparticles; B) MCM-41 calcined nanoparticles, C) S1 solid, D) S1-P solid and E) S2-P solid. TEM images of F) MCM-41 calcined nanoparticles, G) S1-P and H) solid S2-P showing the typical hexagonal porosity of the MCM-41 type mesoporous matrix**.**

Furthermore, presence of the mesoporous structure was also confirmed by TEM analyses (Fig. 1, right). In the representative images, spherical nanoparticles were observed, with a mean diameter of 100 nm (92±9, 109±10 and 103±7 nm for calcined MCM-41, S1-P and S2-P solids respectively) and

the loaded and functionalized S1-P and S2-P solids maintained the initial morphology of the mesoporous silica starting matrix. The typical channels of mesoporous MCM-41 support were easily observed as either alternate black and white stripes or as a pseudo-hexagonal array of pores in the images.

Dynamic light scattering (DLS) studies were also carried out. The results showed particles with a mean diameter of 90±15 nm for the starting calcined MCM-41 nanoparticles and of 122±16 and 114±8 for S1-P and S2-P, respectively (Fig. 2). The dynamic diameter of the functionalized nanoparticles was larger than that of the bare nanoparticles due to the presence of the capping ε-poly-L-lysine polymer.

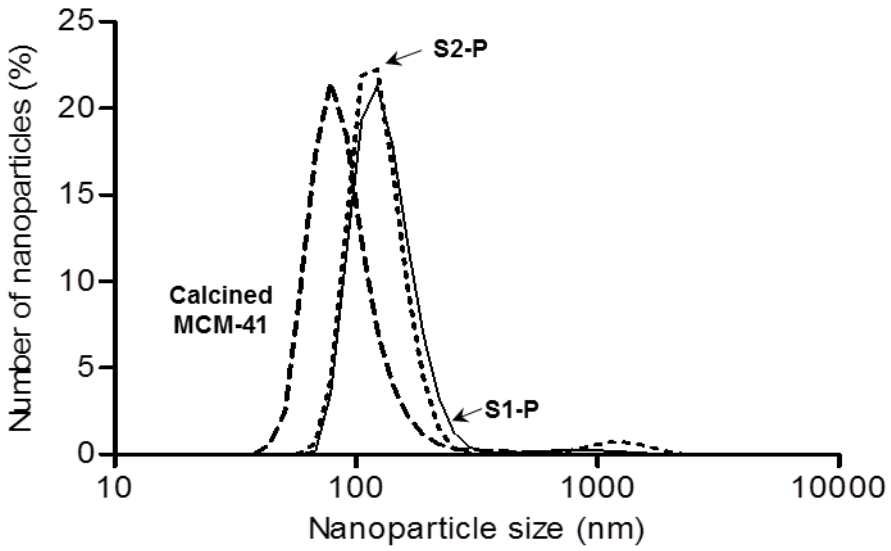

Fig. 2. Size distribution per number of particles obtained by the DLS studies for calcined MCM-41 nanoparticles, S1-P and S2-P.

The N_2 adsorption-desorption isotherm of the MCM-41 calcined nanoparticles is shown in Figure 3. The curve for the starting calcined nanoparticles displays an adsorption step with intermediate P/P_0 values

between 0.1 and 0.3, which correspond to a type IV isotherm that is typical of mesoporous MCM-41-type materials. This step can be related to nitrogen condensation that takes place inside mesopores by capillarity. The specific area was obtained by applying the BET model. From the BJH model on the adsorption curve of the isotherm ($P/P_0 < 0.8$), pore diameter and pore volume were calculated (Table 1). A second feature of the N_2 adsorption-desorption isotherms of the MCM-41 calcined nanoparticles was the characteristic H1 hysteresis loop that appeared on the curve at a high relative pressure ($P/P_0 > 0.8$), which corresponded to the filling of the large pores between nanoparticles due to textural porosity. In this case, curves showed, in addition to the characteristic H1 hysteresis loop, a wide pore size distribution.

For nanoparticles S1-P and S2-P (Fig. 3), the adsorption-desorption isotherms are typical of mesoporous systems with partially filled mesopores and the N_2 volume adsorbed and the specific surface area significantly decrease compared with the starting MCM-41 material (see Table 1).

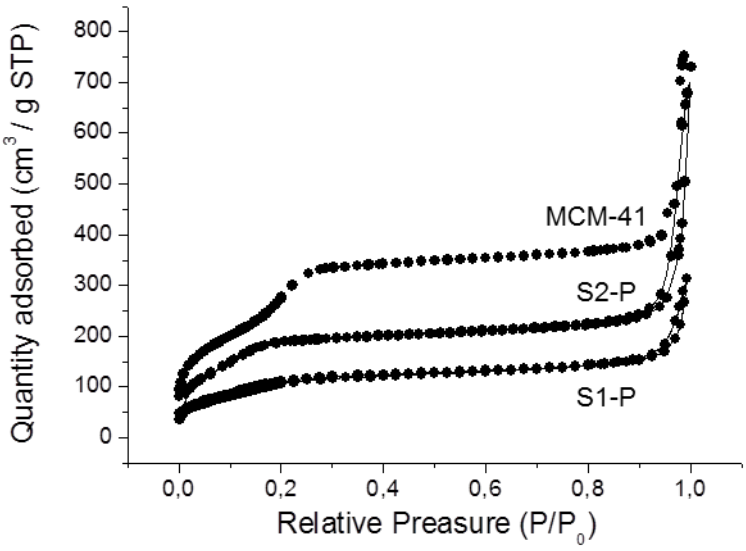

Fig. 3. Nitrogen adsorption-desorption isotherm for: MCM-41 calcined mesoporous nanoparticles, S1-P, and S2-P solids.

Table 1. BET specific surface values, pore volumes and pore sizes calculated from the N_2 adsorption-desorption isotherms for selected materials.

Solid	S_{BET} ($m^2\ g^{-1}$)	Pore volume ($cm^{-3}\ g^{-1}$)	Pore size (nm)
Calcined MCM-41	1020 ± 28	0.63	2.2
S1-P	413 ± 9	0.27	-
S2-P	745 ± 40	0.20	-

The contents of grafted molecules and cargoes in solids S1, S1-P, S2 and S2-P were determined by elemental and thermogravimetric analyses (see Table 2). The isocyanatopropyl contents in solids S2 and S2-P (0.42 mmol/g SiO_2) are nearly the same than those measured for S1 and S1-P solids (0.39 mmol/g SiO_2) and subtle differences in contents could be ascribed to the different grafting and loading process used to prepare the solids (see Experimental section). In the case of the synthesis of S1 and S1-P the loading and the grafting processes were carried out in a one pot fashion using acetonitrile as solvent. On the other hand, solid S2 was loaded with VX-765 in DMSO and then isolated because the functionalization with isocyanatopropyl moieties was carried out in acetonitrile. The amount of polymer in both groups of materials is also quite similar (0.018 g/g SiO_2 for S1-P and 0.014 g/g SiO_2 for S2-P).

Table 2. Content of molecular gate ε-poly-L-Lysine, the isocyanate group and the guest molecule in the different synthesized nanoparticles.

Solid	Rhodamine B mmol/g SiO_2	VX-765 mmol/g SiO_2	NCO mmol/g SiO_2	ε-Poly-L-Lysine g/ g SiO_2
S1	0.33	-	0.39	-
S1-P	0.14	-	0.39	0.018
S2	-	0.14	0.42	-
S2-P	-	0.14	0.42	0.014

Finally, in order to assess the charge of the different prepared nanomaterials (calcined MCM-41, S1, S1-P, S2 and S2-P), the zeta potential were measured. As expected, calcined MCM-41 showed a zeta potential value of -29±1 mV due to the presence of silanolate moieties onto the external surface of the nanoparticles. The rhodamine B loaded solid had a positive value of zeta potential (21±1 mV) induced by the presence of the positively charged dye into the porous network of the nanoparticles. When the external surface of S1 was coated with poly-lysine (soild S1-P) the zeta potential increased to 35±4 mV due to the fact that biopolymer is positively charged at neutral pH. In the case of solid S2, a negative zeta potential was measured (-20±6 mV) probably due to the smaller quantity of VX-765 loaded inside the pores when compared to the rhodamine B presented in S1. Solid S2-P showed a positive zeta potential value (28±5 mV) due to the grafting of poly-lysine onto the external surface of the VX-765-loaded nanoparticles.

3.3. Cargo release studies.

In a first step we tested the controlled release performances of S1-P nanoparticles in water (pH 8.0). In a typical experiment, 1 mg of solid was suspended in 1 mL of water at pH 8.0 in the absence and in the presence of pronase from *Streptomyces griseous*. Aliquots were taken at scheduled times, centrifuged to remove nanoparticles, and the cargo release was evaluated by measuring the emission band of rhodamine B at 575 nm (λ_{ex} = 555 nm). The obtained results are shown in Fig. 4. A poor rhodamine B delivery occurred in the absence of the enzyme (less than 20%), which is indicative of remarkable pore closure (Fig. 4, curve B). Conversely in the presence of pronase pores opened due to the hydrolysis of the peptide bonds in the polymer with the subsequent dye delivery (Fig. 4, curve E). Nearly the same behavior was observed in a highly competitive media such as PBS. As expected, negligible rhodamine B release was observed in the absence of pronase (Fig. 4, curve A) whereas a marked dye delivery was observed when enzyme was present (Fig. 4, curve D). Moreover, to assess the crucial role played by the enzyme in the release mechanism, cargo release for solid S1-P in the presence of denatured pronase was studied. As could be seen in curve C in Fig. 4 a negligible rhodamine B delivery was observed in the presence of denatured pronase. This result demonstrated the specific enzyme response of the gated nanoparticles. Besides, we analysed by HPLC the content of the aliquots obtained at scheduled times after solid S1-P was treated with pronase. HPLC measurements showed the presence of lysine in the aliquots, pointing toward a pronase-induced poly(lysine) hydrolysis as mechanism that governed rhodamine B release (see Supporting information).

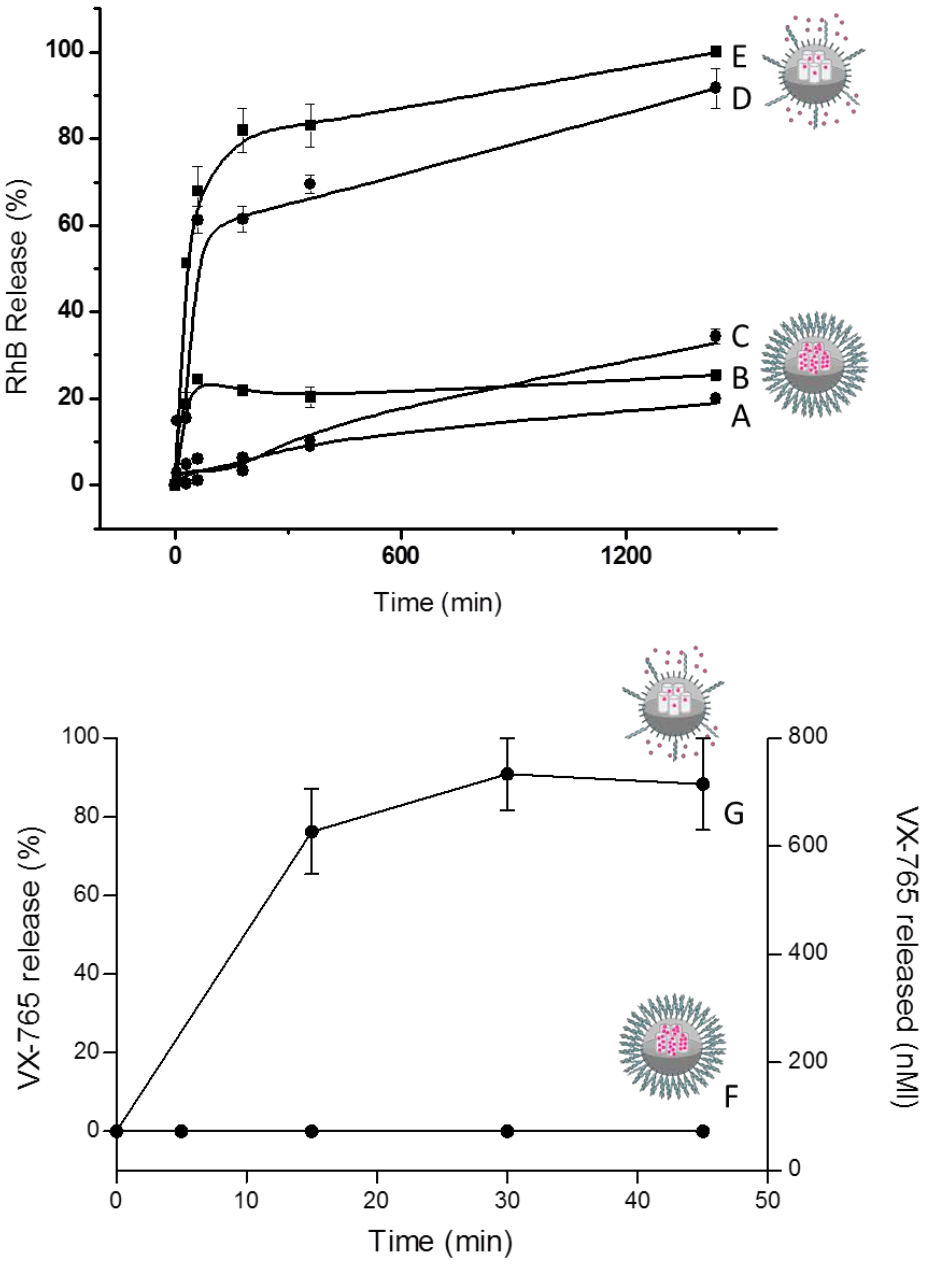

Fig. 4. Top: Enzyme-responsive rhodamine B release form solid S1-P: (A) in the absence of pronase in PBS at pH 7.5; (B) in the absence of pronase in water at pH 8.0; (C) in the presence of denatured pronase in PBS at pH 7.5; (D) in the presence of pronase in PBS at pH 7.5; (E) in the presence of pronase in water at pH 8.0. Down: Enzyme-responsive VX-765 release from solid S2-P in water at pH 8.0 (F) in the absence and (G) in the presence of pronase.

Similar release experiments were carried out with solid S2-P. In this case, delivery of VX-765 from nanoparticles was determined by HPLC analyses. A near-zero release was observed in the absence of pronase, whereas clear drug delivery was detected when enzymes were present (see Fig. 4, curves F and G). The VX-765 concentration reached (after 45 min of pronase addition) was ca. 700 nM, which is a value higher than the IC_{50} reported for this drug (ca. 100 nM). This indicated that relevant therapeutic concentrations of VX-765 can be reached using solid S2-P. The delivery experiments also showed that after 1 h, the VX-765 concentration lowered in the medium (data not shown), which was most likely due to an enzyme-mediated hydrolysis or drug degradation.

As it can also be observed in Fig. 4 an apparent faster payload release was observed for solid S2-P when compared with S1-P in the presence of enzyme and most likely ascribed to the fact that VX-765 is hydrolyzed by the enzyme used to trigger cargo release. This hydrolysis/degradation process of VX-765 avoids the detection of the real maximum delivery peak because after 1 h the amount of payload release began to decrease (the hydrolysis of VX-765 began to be faster than its release from S2-P). This is why maximum VX-765 delivery appears at ca. 30 min. A second potential explanation that may also account for the different payload release observed for solids S1-P (loaded with rhodamine) and S2-P (loaded with VX-765) is, as noted above, the different physical properties of both molecules (such as solubility, polarity, etc). It is well known that delivery from silica mesoporous materials is highly influenced by the nature of the cargo.

3.4. Characterization of ε-poly-L-lysine-capped nanoparticles activity in cellular models of inflammation.

Cytotoxicity and cellular uptake studies with the dye-loaded S1-P nanoparticles in the THP-1 acute monocytic leukemia cell line were carried out as a preliminary step to further characterize S2-P nanoparticles in an *in vivo* anti-inflammatory model (*vide infra*). Cell viability studies that measured mitochondrial activity (WST-1 assays) in the presence of S1-P indicated that nanoparticles were well-tolerated by THP-1 cells at concentrations up to 150 μg/mL (Fig. 5 A) after 6 and 24 h of exposure. Furthermore, a non significant LDH release, indicative of the absence of cellular necrosis or pyroptosis, was observed within the 25-150 μg/mL concentration range (see Fig. 5 B) both for 6 and 24 h of treatments.

To evaluate the cellular uptake of rhodamine B-loaded, ε-poly-L-lysine-capped S1-P solid by THP-1 cells, internalization of nanoparticles was evaluated by flow cytometry and by confocal microscopy (Fig. 5 C and D). These studies demonstrated that up to 80% of the cellular population internalized S1-P 30 min upon treatment, which suggests that these nanoparticles can be used for delivery applications in THP-1 cells. Based on previous published results obtained with similar MSNs capped with enzyme degradable caps [39], it has been postulated that S1-P nanoparticles internalize by endocytosis. The resulting endosomal vesicles would fuse to lysosomes, where the activity of lysosomal enzymes would induce ε-poly-L-lysine hydrolysis and entrapped cargo delivery.

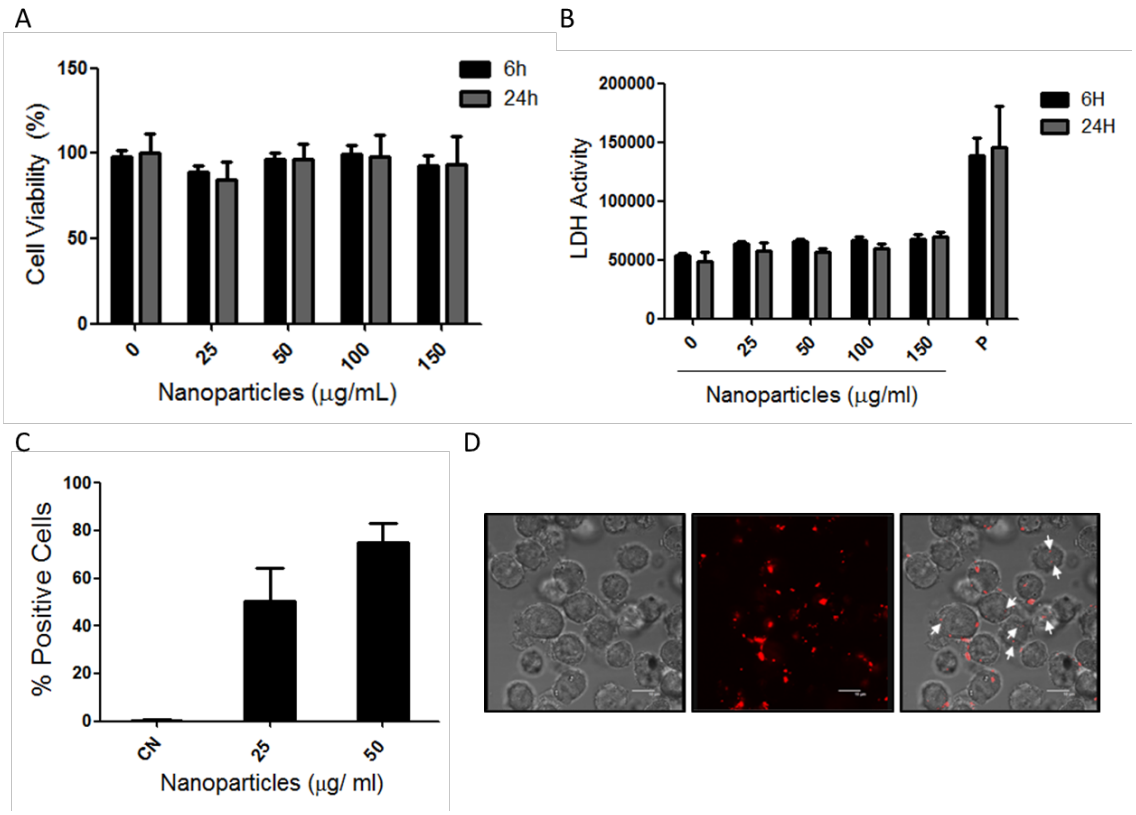

Fig. 5. Cytotoxicity and internalization studies of S1-P at different concentrations of nanoparticles in THP-1 cells. A) Cell viability by the WST-1 assay, B) LDH-activity in the presence of nanoparticles. The positive control of LDH activity (P) was obtained by cellular lysis in 1%Triton-X100 (P) in the absence of nanoparticle. C) Percentage of fluorescent cells analyzed by flow cytometry in internalization studies D) S1-P uptake (in red) by THP-1 cells analyzed by confocal microscopy. Confocal images of cells treated with the S1-P nanoparticle at 50 µg/mL for 1 h. Data represent the mean±SEM of at least three independent experiments.

3.5. Anti-inflammatory activity of S2-P nanoparticles and free VX-765 in a cellular model of inflammation.

After performing internalization studies of S1-P nanoparticles in THP-1 cells, further assays to test the anti-inflammatory activity of the S2-P nanoparticles in the same cell line were carried out. In a first step, it was verified

that stimulation of THP-1 cells with LPS and MDP produced synthesis of pro-IL1-β and activation of pro-caspase-1 by the inflammasome. Under these conditions, an increase in processed IL-1β and activated caspase-1 (casp-1 p20 subunit) in the supernatant of cell cultures was observed (Fig. 6A and B, third line). Treatment of stimulated THP-1 with encapsulated VX-765 (S2-P nanoparticles) at the 50, 75 and 100 µg concentrations of solid/mL, or free VX-765 (1 and 2 µM), diminished the release of both IL-1β and activated caspase-1 to the medium (Fig. 6A and B, lines 5-7 and 8-9, respectively). Fig. 6 shows that the activity of S2-P nanoparticles at a concentration of 100 µg/mL is similar to that obtained using 1 µM of free VX-765. Moreover, the HPLC studies found that a concentration of 100 µg/mL of S2-P corresponded to an equivalent concentration of VX-765 of 13.7 µM (considering that all the encapsulated VX-765 can be released). This indicated that for a similar drug concentration, nanoparticles were less effective than the free drug in assays using THP-1 cells. However, these results strongly contrast with the *in vivo* studies carried out in a mouse model of inflammation in which nanoparticles S2-P displayed much more effective anti-inflammatory activity than the free drug (*vide infra*).

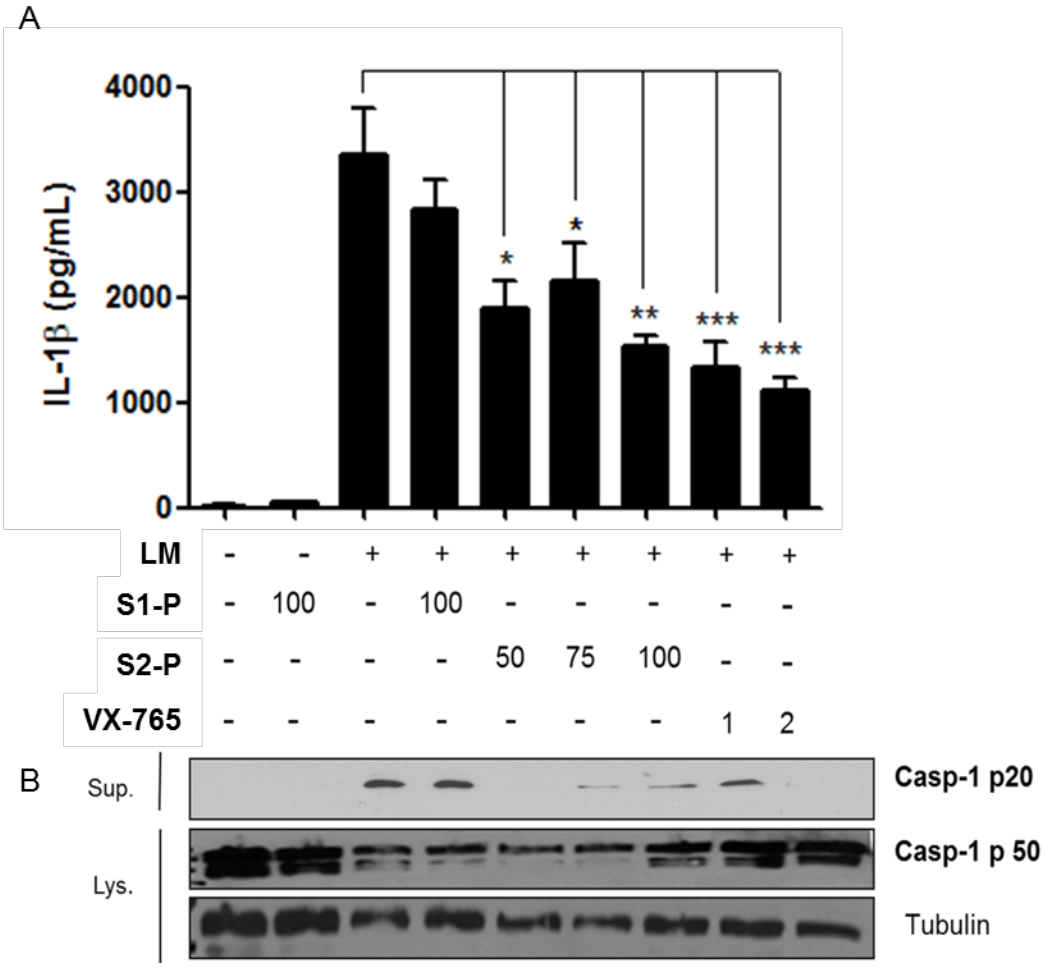

Fig. 6. Inhibition of IL-1β and caspase-1 release induced by S2-P treatment in a cellular model of inflammation. Quantification of inflammatory markers in the THP-1 cells stimulated with LPS+MDP. A) IL-1β Levels from cell supernatants measured by enzyme-linked immunosorbent assay (ELISA). B) Levels of active caspase-1 (p-20) detected in the supernatants, inactive fraction of caspase 1 (p50) in cell lysates and, tubulin in cell lysates as a control by Western Blot. Data represent the mean±SEM of at least three independent experiments (* $p< 0.005$, ** $p<0.0025$, *** $p<0.0001$).

3.6. Anti-inflammatory activity of S2-P nanoparticles and free VX-765 in the *in vivo* model of inflammation.

Having demonstrated the activity of S2-P nanoparticles in cellular assays, we moved one step forward to characterize the anti-inflammatory properties of nanoparticles in an *in vivo* model of inflammation.

In particular, firstly, S2-P activity was evaluated in a subcutaneous air pouch inflammation mouse model. In this model, injection of LPS into the air pouch induced an inflammatory response that was easily quantified by the increase in exudates of inflammatory mediators IL-1β, IL-18, TNF-α and IL-10. To confirm that in the air pouch in vivo model of inflammation, release of IL-1β is dependent of the inflammasome, we have demonstrated caspase-1 activation in the animal exudates by western blot analysis (see Supporting Information Fig. S2). After the intra-pouch administration of free VX-765 at 0.01 mg/kg or S2-P at 0.8 and 1.6 mg/kg (which corresponded to amounts of 0.05 and 0.1 mg/kg of VX-765, respectively) in the mouse model, both inflammasome-dependent interleukins IL-1β and IL-18 significantly reduced in exudates (Fig. 7A and B). The therapeutic effect of VX-765 in all cases was the inhibition of ca. 50% of inflammatory activity, and agreed with the cellular model results. In this case no significant differences in activity were found at similar concentrations of VX-765 free or encapsulated in S2-P. These results corroborated that treatment with VX-765-loaded mesoporous silica nanoparticles S2-P in an animal model was possible and that the inflammatory response properly reduced. In addition, levels of TNF-α and IL-10 were also analyzed as a control of inflammasome-independent cytokines. As expected, no significant differences between the group treated only with LPS and the different treatments with the drug were observed (Fig. 7C and D). These data suggest that a reduction in the IL-1β and IL-18 levels resulted from the specific effect of VX-765 on caspase-1 activity.

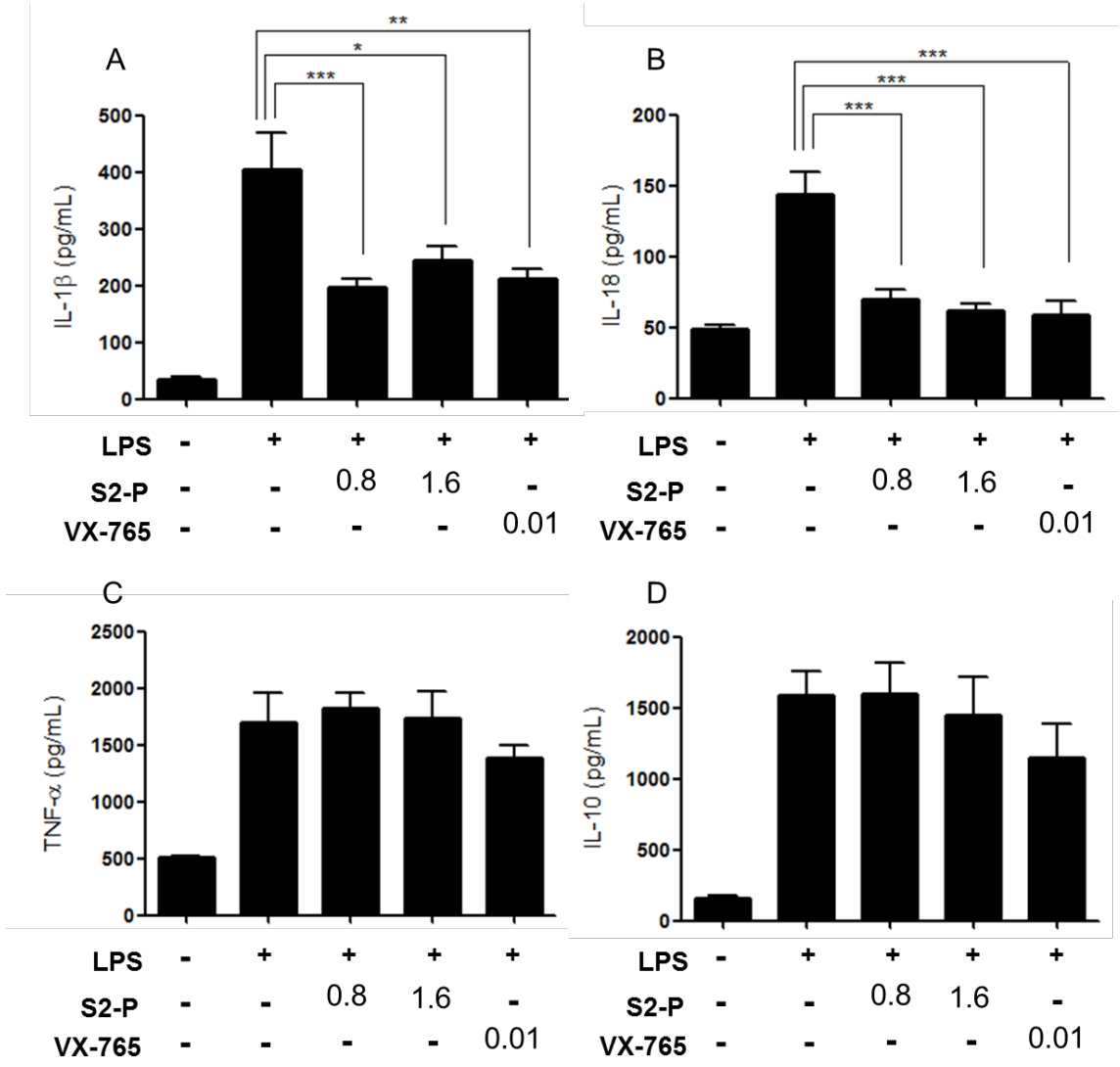

Fig. 7. *In vivo* inhibition of cytokines production by local administration of S2-P. Upon air pouch induction, the mice stimulated with LPS were treated with S2-P at 0.8 and 1.6 mg/kg (which corresponded to 0.05 and 0.1 mg/kg of VX-765, respectively) or with VX-765-free drug (0.01 mg/kg) for 2 h. Then presence of the cytokine in the air pouch exudates was analyzed by ELISA. Quantification of the assays (n=8) for IL-1β, IL-18, TNF-α and IL-10 is showed in A), B), C) and D) panels, respectively. Data represent the mean±SEM of at least three independent experiments (* $p< 0.005$, ** $p<0.0025$, *** $p<0.0001$).

In another step, the activity of VX-765, either free or encapsulated (S2-P), was also analyzed in the same subcutaneous air pouch inflammation mouse model by an intravenous tail injection of VX-765 and S2-P. For the intravenous administration of VX-765, doses were adjusted according to previous reports [56]. As described above, the subcutaneous injection of LPS into the air pouch induced the secretion of IL-1β and IL-18 inflammatory cytokines in exudates. The treatment of LPS-stimulated mice with S2-P at 75 mg/kg i.v. (which corresponded to 4.2 mg/kg of VX-765) or free VX-765 at 10 mg/kg, which clearly reduced inflammatory cytokines levels in both cases. In this systemic approach, significant differences were also observed in the IL-1β and IL-18 release upon treatment with nanoparticles. By taking advantage of drug protection and the preferential systemic distribution of nanoparticles to inflamed tissues, in this case the therapeutic effect of the encapsulated drug upon intravenous administration was noteworthily better than that of the free drug (Fig. 8). In particular, a significant reduction in LPS-induced inflammation (ca. 50% of interleukins inhibition) was observed when S2-P was used, while differences were not significant for the free drug (around 20-25% of inhibition). Note that in these experiments the amount of loaded VX-765 in S2-P (4.2 mg/kg) was lower than the dose of free drug administrated intravenously (10 mg/kg), which indicated that, in this case, VX-765 was almost 4-fold more effective when encapsulated; i.e. the therapeutic effect clearly increased with nanoformulation. These results demonstrated the effectiveness of capped nanoparticles as passively targeted drug delivery systems to inhibit inflammatory response.

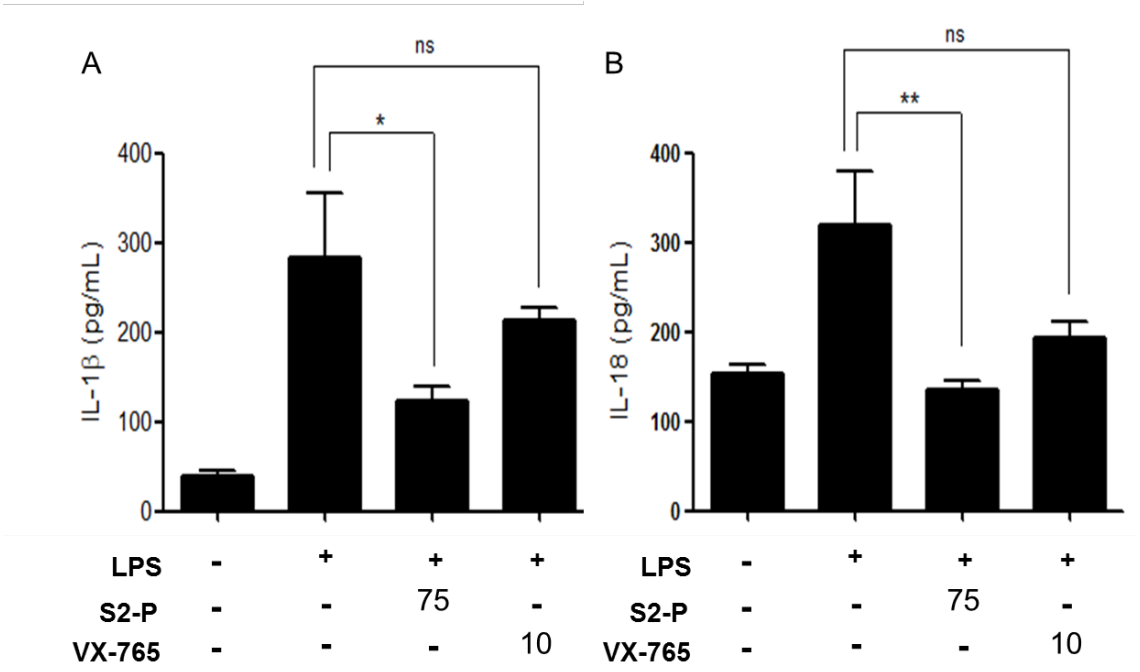

Fig. 8. Anti-inflammatory effects of an intravenous administration of S2-P at 75 mg/kg (corresponds to 4.2 mg/kg of VX-765) in the air pouch inflammation model. IL-1β (A) and IL-18 (B) quantification from the exudates of the systemic assay in the air pouch mouse model in different mice groups (n=8). Data represent the mean±SEM of at least three independent experiments (* $p< 0.005$, ** $p<0.0025$, *** $p<0.0001$).

Analyses of silica content in exudates (Fig. 9) confirmed our hypothesis. Similar background Si levels were detected in mice with no induced inflammation (not treated with LPS) in the exudate samples from the air pouch mouse when no nanoparticles or S2-P were intravenously injected (2.2 and 2.8 µg of Si/ g exudate, respectively). Conversely in the S2-P-treated group (75 mg/kg by intravenous injection), where inflammation was induced by LPS, a clear 2-fold increase in the Si concentration was observed in exudates (5.33 µg of Si/g exudate). These results suggested some specific targeting of nanoparticles at the inflammation focus.

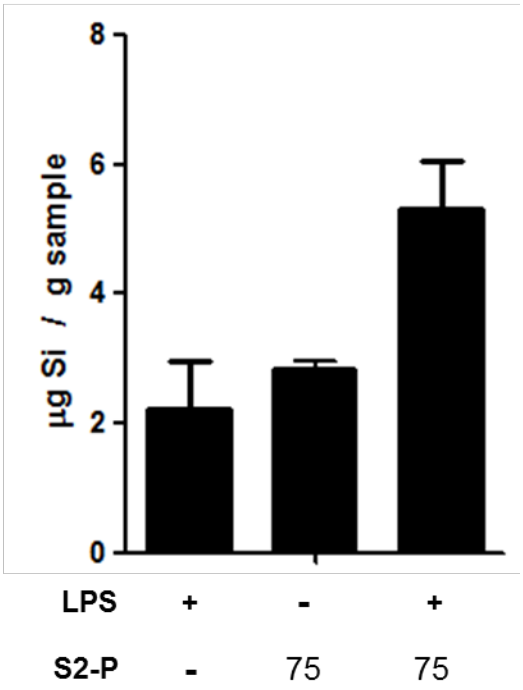

Fig. 9. Silica quantification in the exudate samples from the air pouch mouse. Quantification was performed in groups of mice not submitted to any nanoparticles treatment, S2-P treatment (without LPS) and from the air pouch mouse treated with LPS and S2-P by intravenous injection.

4. Conclusions

Our results demonstrate that delivery of anti-inflammatory drugs using gated mesoporous silica nanoparticles is a suitable tool to develop therapeutic strategies to treat inflammatory diseases. In particular, we developed a drug delivery system to inhibit the inflammatory response in an inflammatory model. The carrier consists in ε-poly-L-lysine-gated mesoporous silica nanoparticles capable of delivering the VX-765 drug in macrophages in *in vitro* and *in vivo* models of inflammation. Our design employs two basic concepts: (a) it is possible to take advantage of the passive targeting of nanoparticles to

macrophages and (b) capped materials can deliver modulators of inflammasome in macrophages present at the inflammation focus. ε-poly-L-lysine-functionalized nanoparticles are efficiently taken up by macrophage cells, most likely via endocytosis, and further reach autolysosomes where the polymer is degraded by lysosomal enzymes and cargo is released. We corroborate that using mesoporous silica nanoparticles in non toxic doses does not trigger an anti-inflammatory response in either macrophages or an *in vivo* air pouch mouse model. We prove that the nanoparticles which encapsulate VX-765 can be intravenously injected into the *in vivo* inflammation model and that the drug is able to reach the inflammation focus. The drug therapeutic effect is enhanced by a significant reduction in the inflammatory response when S2-P is injected, compared with the free drug in the animal model. In particular, VX-765 is ca. 4-fold more effective when encapsulated. The demonstration that gated mesoporous silica materials can release drugs selectively at the inflammatory focus is state of the art and, as far as we know, no similar systems to those described herein to treat inflammatory-based diseases have been reported.

ACKNOWLEDGMENTS. The authors wish to express their gratitude to the Spanish government (Projects MAT2015-64139-C4-1-R and SAF2014-52614-R (MINECO/FEDER)) and the Generalitat Valencia (Projects PROMETEOII/2014/061and PROMETEOII/2014/047) for support. A.G-F. is grateful to the Spanish government for an FPU grant.

References

[1] K. Hoste, K. De Winne, E. Schacht, Polymeric prodrugs, International Journal of Pharmaceutics, 277 (2004) 119-131.
[2] S. Liu, R. Maheshwari, K.L. Kiick, Polymer-Based Therapeutics, Macromolecules, 42 (2009) 3-13.
[3] T. Traitel, R. Goldbart, J. Kost, Smart polymers for responsive drug-delivery systems. , J. Biomater. Sci. Polym. Ed. , 19 (6) (2008) 13.
[4] F. Puoci, F. Iemma, N. Picci, Stimuli-responsive molecularly imprinted polymers for drug delivery: A review, Current Drug Delivery, 5 (2008) 85-96.
[5] F. Siepmann, J. Siepmann, M. Walther, R.J. MacRae, R. Bodmeier, Polymer blends for controlled release coatings, Journal of Controlled Release, 125 (2008) 1-15.
[6] L.S. Nair, C.T. Laurencin, Biodegradable polymers as biomaterials, Progress in Polymer Science (Oxford), 32 (2007) 762-798.
[7] D. Schmaljohann, Thermo- and pH-responsive polymers in drug delivery, Advanced Drug Delivery Reviews, 58 (2006) 1655-1670.
[8] N.K. Mal, M. Fujiwara, Y. Tanaka, Photocontrolled reversible release of guest molecules from coumarin-modified mesoporous silica, Nature, 421 (2003) 350-353.
[9] N.K. Mal, M. Fujiwara, Y. Tanaka, T. Taguchi, M. Matsukata, Photo-switched storage and release of guest molecules in the pore void of coumarin-modified MCM-41, Chemistry of Materials, 15 (2003) 3385-3394.
[10] E. Aznar, M. Oroval, L. Pascual, J.R. Murguía, R. Martínez-Máñez, F. Sancenón, Gated Materials for On-Command Release of Guest Molecules, Chemical Reviews, 116 (2016) 561-718.
[11] B. Zhang, Z. Luo, J. Liu, X. Ding, J. Li, K. Cai, Cytochrome c end-capped mesoporous silica nanoparticles as redox-responsive drug delivery vehicles for liver tumor-targeted triplex therapy in vitro and in vivo, Journal of Controlled Release, 192 (2014) 192-201.
[12] C. Wang, Z. Li, D. Cao, Y.-L. Zhao, J.W. Gaines, O.A. Bozdemir, M.W. Ambrogio, M. Frasconi, Y.Y. Botros, J.I. Zink, J.F. Stoddart, Stimulated Release of Size-Selected Cargos in Succession from Mesoporous Silica Nanoparticles, Angewandte Chemie International Edition, 51 (2012) 5460-5465.
[13] C. Théron, A. Gallud, C. Carcel, M. Gary-Bobo, M. Maynadier, M. Garcia, J. Lu, F. Tamanoi, J.I. Zink, M. Wong Chi Man, Hybrid Mesoporous Silica Nanoparticles with pH-Operated and Complementary H-Bonding Caps as an Autonomous Drug-Delivery System, Chemistry – A European Journal, 20 (2014) 9372-9380.
[14] R. Liu, P. Liao, J. Liu, P. Feng, Responsive Polymer-Coated Mesoporous Silica as a pH-Sensitive Nanocarrier for Controlled Release, Langmuir, 27 (2011) 3095-3099.
[15] Z. Yu, N. Li, P. Zheng, W. Pan, B. Tang, Temperature-responsive DNA-gated nanocarriers for intracellular controlled release, Chemical Communications, 50 (2014) 3494-3497.
[16] J. Croissant, M. Maynadier, A. Gallud, H. Peindy N'Dongo, J.L. Nyalosaso, G. Derrien, C. Charnay, J.-O. Durand, L. Raehm, F. Serein-Spirau, N. Cheminet, T. Jarrosson, O. Mongin, M. Blanchard-Desce, M. Gary-Bobo, M. Garcia, J. Lu, F. Tamanoi, D. Tarn, T.M. Guardado-Alvarez, J.I. Zink, Two-Photon-Triggered Drug Delivery in Cancer Cells Using Nanoimpellers, Angewandte Chemie International Edition, 52 (2013) 13813-13817.
[17] C. de la Torre, A. Agostini, L. Mondragon, M. Orzaez, F. Sancenon, R. Martinez-Manez, M.D. Marcos, P. Amoros, E. Perez-Paya, Temperature-controlled release by changes in the secondary structure of peptides anchored onto mesoporous silica supports, Chemical Communications, 50 (2014) 3184-3186.

[18] C.-H. Lu, I. Willner, Stimuli-Responsive DNA-Functionalized Nano-/Microcontainers for Switchable and Controlled Release, Angewandte Chemie International Edition, 54 (2015) 12212-12235.
[19] C. De La Torre, L. Mondragõn, C. Coll, A. García-Fernández, F. Sancenõn, R. Martínez-Máñez, P. Amorõs, E. Pérez-Payá, M. Orzáez, Caspase 3 Targeted Cargo Delivery in Apoptotic Cells Using Capped Mesoporous Silica Nanoparticles, Chemistry - A European Journal, 21 (2015) 15506-15510.
[20] R. Qian, L. Ding, H. Ju, Switchable Fluorescent Imaging of Intracellular Telomerase Activity Using Telomerase-Responsive Mesoporous Silica Nanoparticle, Journal of the American Chemical Society, 135 (2013) 13282-13285.
[21] J.S. Beck, J.C. Vartuli, W.J. Roth, M.E. Leonowicz, C.T. Kresge, K.D. Schmitt, C.T.W. Chu, D.H. Olson, E.W. Sheppard, S.B. McCullen, J.B. Higgins, J.L. Schlenker, A new family of mesoporous molecular sieves prepared with liquid crystal templates, Journal of the American Chemical Society, 114 (1992) 10834-10843.
[22] G. Kickelbick, Hybrid Inorganic–Organic Mesoporous Materials, Angewandte Chemie International Edition, 43 (2004) 3102-3104.
[23] D. Tarn, C.E. Ashley, M. Xue, E.C. Carnes, J.I. Zink, C.J. Brinker, Mesoporous Silica Nanoparticle Nanocarriers: Biofunctionality and Biocompatibility, Accounts of Chemical Research, 46 (2013) 792-801.
[24] C. Argyo, V. Weiss, C. Bräuchle, T. Bein, Multifunctional Mesoporous Silica Nanoparticles as a Universal Platform for Drug Delivery, Chemistry of Materials, 26 (2014) 435-451.
[25] D. Peer, J.M. Karp, S. Hong, O.C. Farokhzad, R. Margalit, R. Langer, Nanocarriers as an emerging platform for cancer therapy, Nature Nanotechnology, 2 (2007) 751-760.
[26] R.A. Petros, J.M. DeSimone, Strategies in the design of nanoparticles for therapeutic applications, Nat Rev Drug Discov, 9 (2010) 615-627.
[27] V. Wagner, A. Dullaart, A.K. Bock, A. Zweck, The emerging nanomedicine landscape, Nature Biotechnology, 24 (2006) 1211-1217.
[28] F. Sancenón, L. Pascual, M. Oroval, E. Aznar, R. Martínez-Máñez, Gated Silica Mesoporous Materials in Sensing Applications, ChemistryOpen, 4 (2015) 418-437.
[29] K.H. Chen, D.J. Lundy, E.K.W. Toh, C.H. Chen, C. Shih, P. Chen, H.C. Chang, J.J. Lai, P.S. Stayton, A.S. Hoffman, P.C.H. Hsieh, Nanoparticle distribution during systemic inflammation is size-dependent and organ-specific, Nanoscale, 7 (2015) 15863-15872.
[30] N.K. Jain, V. Mishra, N.K. Mehra, Targeted drug delivery to macrophages, Expert Opinion on Drug Delivery, 10 (2013) 353-367.
[31] O.M. Koo, I. Rubinstein, H. Onyuksel, Role of nanotechnology in targeted drug delivery and imaging: a concise review, Nanomedicine: Nanotechnology, Biology and Medicine, 1 (2005) 193-212.
[32] S.P. Vyas, M.E. Kannan, S. Jain, V. Mishra, P. Singh, Design of liposomal aerosols for improved delivery of rifampicin to alveolar macrophages, International Journal of Pharmaceutics, 269 (2004) 37-49.
[33] S. Chono, T. Tanino, T. Seki, K. Morimoto, Efficient drug targeting to rat alveolar macrophages by pulmonary administration of ciprofloxacin incorporated into mannosylated liposomes for treatment of respiratory intracellular parasitic infections, Journal of Controlled Release, 127 (2008) 50-58.
[34] M. Nahar, N.K. Jain, Preparation, Characterization and Evaluation of Targeting Potential of Amphotericin B-Loaded Engineered PLGA Nanoparticles, Pharmaceutical Research, 26 (2009) 2588-2598.

[35] R. Kalluru, F. Fenaroli, D. Westmoreland, L. Ulanova, A. Maleki, N. Roos, M. Paulsen Madsen, G. Koster, W. Egge-Jacobsen, S. Wilson, H. Roberg-Larsen, G.K. Khuller, A. Singh, B. Nyström, G. Griffiths, Poly(lactide-co-glycolide)-rifampicin nanoparticles efficiently clear Mycobacterium bovis BCG infection in macrophages and remain membrane-bound in phago-lysosomes, Journal of Cell Science, 126 (2013) 3043-3054.
[36] J. Pruthi, N.K. Mehra, N.K. Jain, Macrophages targeting of amphotericin B through mannosylated multiwalled carbon nanotubes, Journal of Drug Targeting, 20 (2012) 593-604.
[37] V.K. Prajapati, K. Awasthi, S. Gautam, T.P. Yadav, M. Rai, O.N. Srivastava, S. Sundar, Targeted killing of Leishmania donovani in vivo and in vitro with amphotericin B attached to functionalized carbon nanotubes, Journal of Antimicrobial Chemotherapy, 66 (2011) 874-879.
[38] D.L. Clemens, B.-Y. Lee, M. Xue, C.R. Thomas, H. Meng, D. Ferris, A.E. Nel, J.I. Zink, M.A. Horwitz, Targeted Intracellular Delivery of Antituberculosis Drugs to Mycobacterium tuberculosis-Infected Macrophages via Functionalized Mesoporous Silica Nanoparticles, Antimicrobial Agents and Chemotherapy, 56 (2012) 2535-2545.
[39] J. Xie, D. Xiao, J. Zhao, N. Hu, Q. Bao, L. Jiang, L. Yu, Mesoporous Silica Particles as a Multifunctional Delivery System for Pain Relief in Experimental Neuropathy, Advanced Healthcare Materials, (2016) n/a-n/a.
[40] F. Krombach, S. Münzing, A.M. Allmeling, J.T. Gerlach, J. Behr, M. Dörger, Cell size of alveolar macrophages: an interspecies comparison, Environmental Health Perspectives, 105 (1997) 1261-1263.
[41] P.J. Murray, T.A. Wynn, Protective and pathogenic functions of macrophage subsets, Nat Rev Immunol, 11 (2011) 723-737.
[42] R. Medzhitov, C.A. Janeway Jr, Innate Immunity: The Virtues of a Nonclonal System of Recognition, Cell, 91 (1997) 295-298.
[43] M. Keller, A. Rüegg, S. Werner, H.-D. Beer, Active Caspase-1 Is a Regulator of Unconventional Protein Secretion, Cell, 132 (2008) 818-831.
[44] F. Martinon, K. Burns, J. Tschopp, The Inflammasome: A Molecular Platform Triggering Activation of Inflammatory Caspases and Processing of proIL-β, Molecular Cell, 10 (2002) 417-426.
[45] K. Schroder, J. Tschopp, The Inflammasomes, Cell, 140 (2010) 821-832.
[46] T. Bergsbaken, S.L. Fink, B.T. Cookson, Pyroptosis: host cell death and inflammation, Nat Rev Micro, 7 (2009) 99-109.
[47] S.L. Fink, B.T. Cookson, Caspase-1-dependent pore formation during pyroptosis leads to osmotic lysis of infected host macrophages, Cellular Microbiology, 8 (2006) 1812-1825.
[48] T. Strowig, J. Henao-Mejia, E. Elinav, R. Flavell, Inflammasomes in health and disease, Nature, 481 (2012) 278-286.
[49] W. Wannamaker, R. Davies, M. Namchuk, J. Pollard, P. Ford, G. Ku, C. Decker, P. Charifson, P. Weber, U.A. Germann, K. Kuida, J.C.R. Randle, (S)-1-((S)-2-{[1-(4-Amino-3-chloro-phenyl)-methanoyl]-amino}-3,3-dimethyl-butanoyl)-pyrrolidine-2-carboxylic acid ((2R,3S)-2-ethoxy-5-oxo-tetrahydro-furan-3-yl)-amide (VX-765), an Orally Available Selective Interleukin (IL)-Converting Enzyme/Caspase-1 Inhibitor, Exhibits Potent Anti-Inflammatory Activities by Inhibiting the Release of IL-1β and IL-18, Journal of Pharmacology and Experimental Therapeutics, 321 (2007) 509-516.
[50] J.H. Stack, K. Beaumont, P.D. Larsen, K.S. Straley, G.W. Henkel, J.C.R. Randle, H.M. Hoffman, IL-Converting Enzyme/Caspase-1 Inhibitor VX-765 Blocks the Hypersensitive Response to an Inflammatory Stimulus in Monocytes from Familial

Cold Autoinflammatory Syndrome Patients, The Journal of Immunology, 175 (2005) 2630-2634.
[51] C. Jakobs, E. Bartok, A. Kubarenko, F. Bauernfeind, V. Hornung, Immunoblotting for Active Caspase-1, in: M.C. De Nardo, E. Latz (Eds.) The Inflammasome: Methods and Protocols, Humana Press, Totowa, NJ, 2013, pp. 103-115.
[52] D.B. Duarte, M.R. Vasko, J.C. Fehrenbacher, Models of Inflammation: Carrageenan Air Pouch, in: Current Protocols in Pharmacology, John Wiley & Sons, Inc., 2001.
[53] V. Escrig, A. Ubeda, M.L. Ferrandiz, J. Darias, J.M. Sanchez, M.J. Alcaraz, M. Paya, Variabilin: A Dual Inhibitor of Human Secretory and Cytosolic Phospholipase A2 With Anti-inflammatory Activity, Journal of Pharmacology and Experimental Therapeutics, 282 (1997) 123-131.
[54] A. Araico, M.C. Terencio, M.J. Alcaraz, J.N. Domínguez, C. León, M.L. Ferrándiz, Evaluation of the anti-inflammatory and analgesic activity of Me-UCH9, a dual cyclooxygenase-2/5-lipoxygenase inhibitor, Life Sciences, 80 (2007) 2108-2117.
[55] L. Mondragón, N. Mas, V. Ferragud, C. De La Torre, A. Agostini, R. Martínez-Máñez, F. Sancenón, P. Amorós, E. Pérez-Payá, M. Orzáez, Enzyme-responsive intracellular-controlled release using silica mesoporous nanoparticles capped with ε-poly- L -lysine, Chemistry - A European Journal, 20 (2014) 5271-5281.
[56] C. Thomas, M.B. Boxer, Caspase inhibitors, in, Google Patents, 2011.